

Probing the Growth and Aging of Colloidal Cobalt Nanocrystals: A Combined Study by Transmission Electron Microscopy and Magnetic Measurements

Guangjun Cheng,^{*,†} Cindi L. Dennis,[‡] Robert D. Shull,[‡] and A. R. Hight Walker[†]

Optical Technology Division, Physics Laboratory, National Institute of Standards and Technology, Gaithersburg, Maryland 20899, and Metallurgy Division, Materials Science and Engineering Laboratory, National Institute of Standards and Technology, Gaithersburg, Maryland 20899

Received April 15, 2009; Revised Manuscript Received May 21, 2009

ABSTRACT: We have combined transmission electron microscopy (TEM) and magnetic measurements to probe the growth and aging of colloidal cobalt (Co) nanocrystals and demonstrated that these two techniques together yield structure and property information in a manner that neither can do alone. During the growth, TEM shows the formation of Co nanocrystals ($4.8 \text{ nm} \pm 1.7 \text{ nm}$), while magnetic measurements indicate the presence of paramagnetic Co cluster complexes and weakly interacting Co nanocrystals. At the completion of the synthesis, TEM shows that the average size of the Co nanocrystals has increased, but with a narrower size distribution ($10.5 \text{ nm} \pm 1.0 \text{ nm}$). Meanwhile, magnetic measurements demonstrate the strong interactions between the Co nanocrystals. Exchange bias and increased coercivity are observed for the aged Co colloid under field-cooled conditions, indicating the existence of antiferromagnetic/ferromagnetic (AFM/FM) coupling. High-resolution TEM confirms that AFM face-centered cubic cobalt(II) oxide grows on the surface of the FM ϵ -Co nanocrystals, but this oxide layer is thin and inhomogeneous. These combined results suggest that not only the AFM/FM exchange coupling within individual aged nanocrystal matters but also the strong magnetostatic coupling between the neighboring nanocrystals significantly contributes to the observed exchange bias.

Introduction

Chemically synthesized nanocrystals have numerous applications in areas such as electronics, optics, catalysis and medicine.^{1–3} Therefore, it is important to probe the growth mechanisms of these nanocrystals and their aging after synthesis. By applying multiple characterization techniques and correlating these measurements with the properties of these nanocrystals,⁴ a protocol can be established to characterize the system effectively and rapidly. In addition, the combined information will provide researchers a comprehensive view of the synthesized nanocrystals. A successful example is the case of photonic nanocrystals. The growth kinetics of the colloidal semiconductor nanocrystals have been investigated by combining several characterization techniques including transmission electron microscopy (TEM), ultraviolet–visible (UV–vis) spectroscopy, and photoluminescence (PL) spectroscopy, and then correlating the UV–vis and PL peaks with the sizes of the nanocrystals determined from TEM measurements.⁵ The aging of colloidal gold nanocrystals and their reduced reactivity in ligand exchange reactions have been studied by TEM, UV–vis spectroscopy, and thermal analysis, indicating a surface reorganization during the aging of these nanocrystals.⁶ Compared with the optical measurements for these photonic nanocrystals, magnetic measurements can be a powerful way to study the growth and aging of magnetic nanocrystals.^{7–10}

Since its discovery,^{11–14} the thermal decomposition of dicobalt octacarbonyl ($\text{Co}_2(\text{CO})_8$) under inert atmospheric conditions in the presence of surfactants has been used to synthesize cobalt (Co) nanocrystals with controlled size, shape, and crystal structure. These colloidal nanocrystals have been widely used in the fields of nanocrystal synthesis,¹⁵ magnetism,¹⁶ catalysis,¹⁷ and biology.¹ The growth and aging of Co nanocrystals involve

the decomposition of $\text{Co}_2(\text{CO})_8$ and the oxidization of these nanocrystals, thus providing a rich system for magnetic measurements. TEM has typically been used to monitor the growth of Co nanocrystals.^{12,14} Recently, Fourier transform infrared spectroscopy (FTIR)^{18–20} and electrospray ionization mass spectrometry (ESI-MS)^{21,22} have been used to identify the intermediates produced during the growth of Co nanocrystals. To our knowledge, magnetic measurements have not yet been used to investigate this growth colloid. In terms of the stability of Co nanocrystals with respect to oxidation, magnetic measurements have demonstrated that their stability is strongly dependent on the surfactants used in synthesis and X-ray diffraction has shown that cobalt(II) oxide (CoO) or cobalt(II, III) oxide (Co_3O_4) forms after thermal annealing.²³ Meanwhile, the magnetic measurements on the purposefully oxidized Co nanocrystals have revealed that the thickness of antiferromagnetic (AFM) CoO, growing on the surface of ferromagnetic (FM) Co nanocrystals, strongly affects the AFM/FM coupling and exchange bias observed.^{24,25} However, in those measurements, Co nanocrystals are intentionally oxidized and measured in their dry powder form.

In this paper, we have combined TEM and magnetic measurements to systematically characterize the growth colloid and the freshly prepared and then aged Co colloid, which were prepared in the presence of surfactants, oleic acid (OA) and trioctylphosphine oxide (TOPO). These three colloids are used to monitor the magnetic behavior of these nanocrystals in frozen and liquid carrier, which is particularly critical for the investigations of their interactions and their magnetic field-induced assemblies.^{26,27} The magnetic measurements include hysteresis loops and a series of magnetic moment vs temperature (m vs T) measurements. In order to probe their growth intermediates, Co nanocrystals are synthesized using a two-step process by modifying the typical one-step synthesis.^{26–28} Instead of injecting the Co precursor solution and performing the synthesis at the same temperature in the one-step synthesis, the Co precursor

* Corresponding author. E-mail: guangjun.cheng@nist.gov. Tel: (301)-975-5209. Fax: (301)-975-6991.

[†] Optical Technology Division, Physics Laboratory.

[‡] Metallurgy Division, Materials Science and Engineering Laboratory.

was injected at a lower temperature and then the reaction was continued at a higher temperature. The growth colloid collected at a lower reaction temperature was used for TEM and magnetic measurements to investigate the growth intermediates of the Co nanocrystals, while the colloid collected at the completion of the synthesis was used to characterize the final product and track its aging process. We would like to point out that, in our aging study, these colloidal nanocrystals were still immersed in their liquid carrier and the colloid was stored in air at room temperature. No extra oxygen or heat treatment was provided since our intent was to probe the natural aging of these colloidal nanocrystals and provide critical information for their further applications. High-resolution TEM (HRTEM) and magnetic measurements were used to study colloidal Co nanocrystals during aging. Exchange bias due to the surface oxidation of the Co nanocrystals was observed, and the significant contribution from the strong interactions between neighboring nanocrystals in this effect is discussed herein. The results demonstrate the power of combining these two techniques to explore the natural oxidization of colloidal cobalt nanocrystals and their interactions.

Experimental Section

Chemicals. Dicobalt octacarbonyl containing 1% to 5% hexane as a stabilizer, oleic acid (OA, 99%), and 1,2-dichlorobenzene (DCB, 99%, anhydrous) were purchased from Aldrich (Milwaukee, WI). Trioctylphosphine oxide (TOPO, 90%) was purchased from Alfa Aesar (Ward Hill, MA). All chemicals were used without further treatment.

Synthesis of Co Nanocrystals. Co nanocrystals were synthesized using a two-step process. First, 0.25 g of TOPO and 0.1 mL of OA were degassed in argon (Ar) in a flask for 20 min. Then 12 mL of DCB was introduced into the flask under an Ar atmosphere. The solution was heated to 393 K, and ~ 0.5 g of $\text{Co}_2(\text{CO})_8$ dissolved in 3 mL of DCB was quickly injected into the mixture. The reaction continued for 10 min, and then 1 mL of colloid was extracted using an airtight syringe and stored in a glass vial under argon (Co1 colloid). The mixture was then heated to the reflux temperature of DCB (~ 453 K), the reaction was continued for 10 min, and then the colloid was extracted using an airtight syringe and stored in a glass vial under argon (Co2 colloid). The weight percentage of Co nanocrystals in Co2 colloid is approximately 1%.

TEM Characterization. Images of the nanocrystals from Co1 and Co2 colloids were obtained on a HITACHI H-600 transmission electron microscope (100 kV). HR-TEM images for the aged Co2 colloid were obtained on a JEOL-2100 LaB₆ TEM (200 kV). TEM samples were prepared by dropping the colloids onto carbon-coated TEM grids (Formvar/Carbon Cu grids, purchased from Ted Pella, Inc. Redding, CA) and allowing the DCB to evaporate in air.

Magnetic Characterization. A superconducting quantum interference device (SQUID, Quantum Design MPMS) magnetometer was used to measure the magnetic properties of Co1 and Co2 colloids. The colloids were loaded into screw-sealed Kel-F sample holders (purchased from Lake Shore Cryotronics, Inc., Westerville, OH) for magnetic measurements. While the Co1 colloid was measured within one day, the Co2 colloid was stored in air and measured three times over a period of 116 days after synthesis: on day 2, day 48, and day 116.

Results and Discussion

Figure 1A shows a TEM image of Co nanocrystals from the Co1 colloid extracted 10 min after injecting the Co precursor solution at 393 K. It clearly shows that Co nanocrystals have been produced at this stage, though their sizes are not uniform. The average diameter of the nanocrystals visible in the TEM images is determined to be 4.8 nm with a standard deviation of 1.7 nm as shown in the histogram in Figure 1A. Figure 1B shows a TEM image of Co2 colloidal nanocrystals extracted 10 min after the reaction temperature was raised from 393 to 453 K. Like the freshly prepared Co nanocrystals using the one-

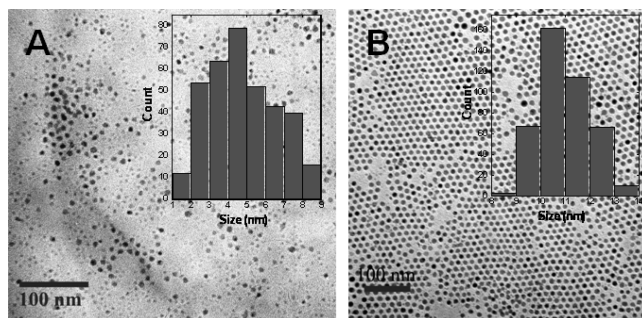


Figure 1. TEM images of (A) Co1 nanocrystals and (B) freshly prepared Co2 nanocrystals. Insets are their size distributions.

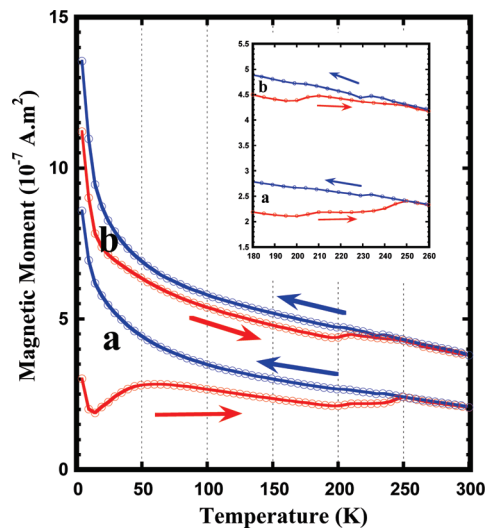


Figure 2. Sequential m vs T measurements from a to b with an applied external magnetic field of (a) 15.9 kA/m (200 Oe) and (b) 39.8 kA/m (500 Oe) for the Co1 colloid. The right-pointing arrows indicate the curves measured during warming, and the left-pointing arrows the curves measured during cooling.

step synthesis,²⁶ the freshly prepared Co nanocrystals here are monodisperse and form a two-dimensional hexagonal array during drying on the TEM grid. The average size of the freshly prepared nanocrystals is determined to be 10.5 nm with a standard deviation of 1.0 nm as shown in the histogram in Figure 1B. The selected-area electron diffraction pattern shows that these nanocrystals also adopt the ϵ -Co structure (data not shown).

In our previous work,²⁶ we carried out the magnetic measurements using a series of m vs T measurements, with and without an external magnetic field, to investigate how the dipolar chains of Co nanocrystals in DCB change under the influence of external magnetic fields. Similar m vs T measurements have been performed for the Co1 and Co2 colloids. The colloids were first cooled to 4.2 K in zero field, followed by applying an external magnetic field of 15.9 kA/m (200 Oe), and then the magnetic moment was measured during warming from 4.2 to 300 K (indicated by the right-pointing arrow) and subsequent cooling from 300 to 4.2 K (indicated by the left-pointing arrow). Then, an external magnetic field of 39.8 kA/m (500 Oe) was applied, and the measurements were repeated during warming and cooling. Figure 2 shows the m vs T measurements for the Co1 colloid, while Figure 3A shows the m vs T measurements for Co2 colloid on day 2 after synthesis. Due to the similar size and size distribution of nanocrystals and the same liquid

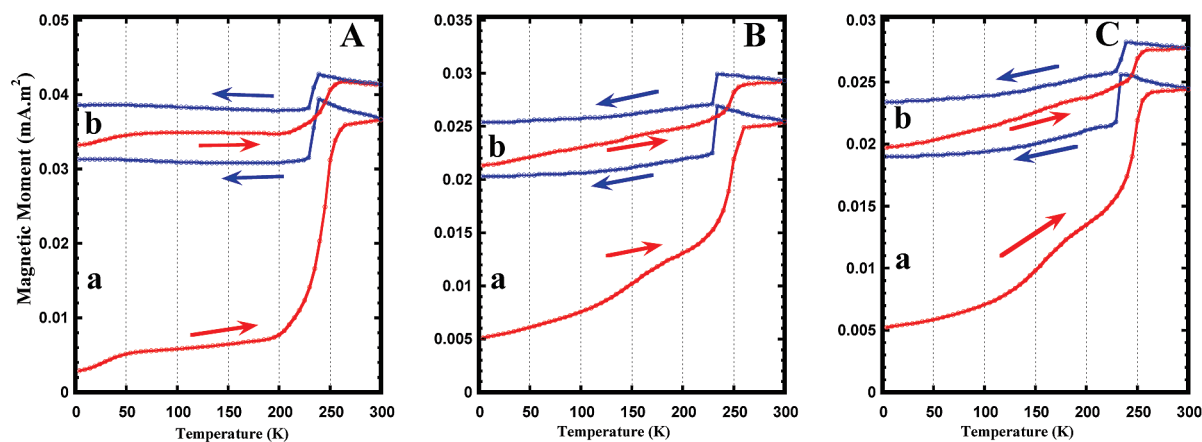


Figure 3. Sequential m vs T measurements from a to b with an applied external magnetic field of (a) 15.9 kA/m (200 Oe) and (b) 39.8 kA/m (500 Oe) for the Co₂ colloid measured on (A) day 2, (B) day 48, and (C) day 116, after synthesis. The right-pointing arrows indicate the curves measured during warming, and left-pointing arrows the curves measured during cooling.

carrier, the m vs T measurements for the Co₂ colloid on day 2 are similar to the ones for the Co colloid using the one-step synthesis method.²⁶ The rapid rise in magnetic moment at 250 K in the heating curve and the discontinuous drop at 234 K in the cooling curve are due to the melting and supercooling of the DCB, respectively.²⁶

The m vs T measurements for the Co₁ colloid in Figure 2 are clearly different from the ones for the Co₂ colloid on day 2 in Figure 3A. A close comparison between these two magnetic behaviors reveals different compositions and morphologies in these two colloids.

First, a broad peak in the warming curve a in Figure 2 for the Co₁ colloid was observed around 60 K. Such a peak is conventionally attributed to the blocking temperature of non-interacting superparamagnetic nanocrystals.^{8,10} In our earlier work, we have shown that chains exist in colloids with 10 nm Co nanocrystals even in zero applied field due to the strong dipolar coupling between the nanocrystals. In the Co₁ colloid, the average size of Co nanocrystals is much smaller (4.8 nm). The dipolar coupling constant for the Co₁ nanocrystals is estimated to be 0.3, much smaller than the required value of 2 for the formation of dipolar chains.^{29,30} Also the particle density in the Co₁ colloid is low at this stage because the Co intermediates have not been fully converted into Co nanocrystals. Therefore, in the Co₁ colloid, these nanocrystals interact weakly with each other, compared with the ones in the Co₂ colloid. Furthermore, the large breadth of the peak seen is probably indicative of the wide size distribution of Co nanocrystals in the Co₁ colloid (35% polydispersity).^{8,10}

Second, the rapid rise in magnetic moment around 250 K during warming and the abrupt drop in magnetic moment at 234 K during cooling observed for the Co₂ colloid in Figure 3A were not observed in Figure 2 for the Co₁ colloid, suggesting that strong particle interactions and their resulting dipolar chains are critical for the rapid rise and abrupt drop observed in the Co₂ colloid. However, both the Co₁ and Co₂ (measured on day 2) colloids show an increase in their magnetic moment at 200 K. This temperature is 50 K below the melting point of DCB, indicating that the Brownian motion of these nanocrystals embedded in frozen DCB may start much earlier than the melting of the bulk liquid carrier.

It has been reported that the thermal motion of individual magnetic nanocrystals and the local wiggling of the individual nanocrystals in a dipolar chain can take place well below the melting point of the liquid carrier.³¹ These early motions were

attributed to the thick polymer coating layer (~7 nm) on these magnetic nanocrystals, which has a significantly lower glass transition point than the melting point of the liquid carrier, thus providing a nonfrozen environment for these nanocrystals in the macroscopically frozen liquid carrier. In contrast, here, the possible coating layer on the Co nanocrystals is a thin organic layer of OA/TOPO (~2 nm). The melting points of OA and TOPO are 286 and 323 K, respectively, much higher than the melting point of the liquid carrier. Despite this, our results clearly show that these nanocrystals, regardless of interaction strength, start their thermal motion before the bulk liquid carrier melts. Therefore, the initial melting of DCB probably starts around Co nanocrystals in the colloid, resulting in a local viscosity change around the Co nanocrystals and enabling their thermal motion. Further evidence is provided by the increase in magnetic moment starting at 200 K in the warming curves at the higher field in Figures 2 and 3A. However, as the temperature further increases, the magnetic moment for Co₁ colloidal nanocrystals decreases as thermal energy demagnetizes these smaller nanocrystals, while the magnetic moment for Co₂ colloidal nanocrystals keeps increasing due to the increased alignment with the magnetic field for these larger, strongly interacting nanocrystals.²⁶

Third, there appears to be a paramagnetic component in the Co₁ colloid. In the warming curves in Figure 2, the magnetic moment decreases rapidly as the temperature rises from 4.2 to 15 K, while the magnetic moment increases rapidly in the cooling curves as the temperature decreases from 15 to 4.2 K. This raises the question about which components in the Co₁ colloid are responsible for this paramagnetic behavior.

It is well established that the thermal decomposition of Co₂(CO)₈ into Co nanocrystals proceeds via the intermediate state of tetracobalt dodecacarbonyl (Co₄(CO)₁₂).^{18–20} FTIR spectra show that the decomposition of Co₄(CO)₁₂ is complete after 2–3 weeks at room temperature.¹⁸ Here, the Co₁ colloid was removed from the reaction after 10 min at 393 K. Therefore, it is reasonable to assume that the intermediate state Co₄(CO)₁₂ may exist in this growth colloid and that this intermediate state remains present in the colloid during the magnetic measurements.

However, the intermediate state Co₄(CO)₁₂ is diamagnetic because all the electrons are paired,³² and thus cannot be responsible for the paramagnetic behavior observed. We have shown that Co nanocrystals have been produced at this stage. Therefore, the nucleation and growth of Co nanocrystals happens before the full decomposition of Co₄(CO)₁₂, and it is reasonable

to assume that there exist other Co components, which link the conversion from $\text{Co}_4(\text{CO})_{12}$ to Co nanocrystals. In fact, recent studies have shown that the reaction product of $\text{Co}_2(\text{CO})_8$ decomposition in DCB depends on the concentration of the oleic acid ligand.^{21,22} With a high concentration of OA, stable Co cluster complexes are formed. The formation of cluster complexes and nanocrystals is interchangeable with the addition or removal of OA from the reaction products. ESI-MS measurements have shown that these cluster complexes are charged Co clusters coordinated with surfactants. Magnetic measurements on these Co cluster complexes have shown that they exhibit paramagnetic behavior.²¹ Therefore, in the Co1 colloid, these Co cluster complexes are most likely responsible for the paramagnetic behavior we observed in Figure 2.

So far, we have shown that, even in just one growth colloid, the different components including diamagnetic $\text{Co}_4(\text{CO})_{12}$, paramagnetic cobalt clusters, and weakly interacting Co nanocrystals are present. As the reaction proceeds from Co1 to Co2, the paramagnetic behavior and broad peak around 60 K completely disappear in the m vs T measurements as shown in Figure 3A, indicating that $\text{Co}_4(\text{CO})_{12}$, Co cluster complexes, and small, weakly interacting Co nanocrystals have been converted into larger, strongly interacting Co nanocrystals. Figures 3B and 3C show the m vs T measurements for the Co2 colloid measured on day 48 and day 116, respectively. Obviously, for the same temperature and magnetic field, as the sample ages, the magnetic moment decreases; furthermore, no paramagnetic behavior is observed in the low temperature region (between 4.2 and 15 K) for the aged Co2 colloid. This is in contrast to Co colloids using the one-step synthesis method, where, over 70 days, Ostwald ripening occurs through the leaching of Co atoms or ions into the liquid carrier (indicated by the appearance of a purple color), resulting in both a decrease in the magnetic moment and the appearance of paramagnetic behavior in the m vs T curves.²⁶ This atom/ion leaching was reported to be a key issue in evaluating the catalytic performance of the transition-metal nanocrystals, especially in the case of palladium nanocrystals.^{33–35} However, the aged Co2 colloid here does not exhibit any color change even over 116 days, indicating no detectable Co leaching and further supporting the premise that multiple techniques must be combined in order to fully characterize a nanocrystal system. Though these two colloids are very similar in terms of their morphology and crystalline structure, the average size of the Co nanocrystals produced using the two-step synthesis method is a little bit larger than those produced using the one-step synthesis method (10.5 nm vs 10.0 nm), but with a smaller relative standard deviation (9.5% vs 14%). Both of these factors could slow down the Co leaching, but should not stop it. Therefore, the growth condition of these nanocrystals also plays an important role in their aging process. In these two syntheses, the surfactant layers probably coat the surface of the freshly prepared nanocrystals differently in terms of packing density and the ratio between OA and TOPO due to the different temperature settings, thereby affecting Co solvation and leaching. In the two-step synthesis, the coating layer prevents Co leaching from the nanocrystals, while in the one-step synthesis, the coating layer promotes leaching.

The decrease in magnetic moment over time is also observed quite clearly in the hysteresis loops at 5 and 298 K for the Co2 colloid measured on day 2, day 48, and day 116, as shown in Figure 4. The saturation magnetic moment at 5 and 298 K decreases as the Co2 colloid ages, which is consistent with the trend in the m vs T measurements in Figure 3. Figure 5 summarizes the magnetic moment for Co2 as a function of aging

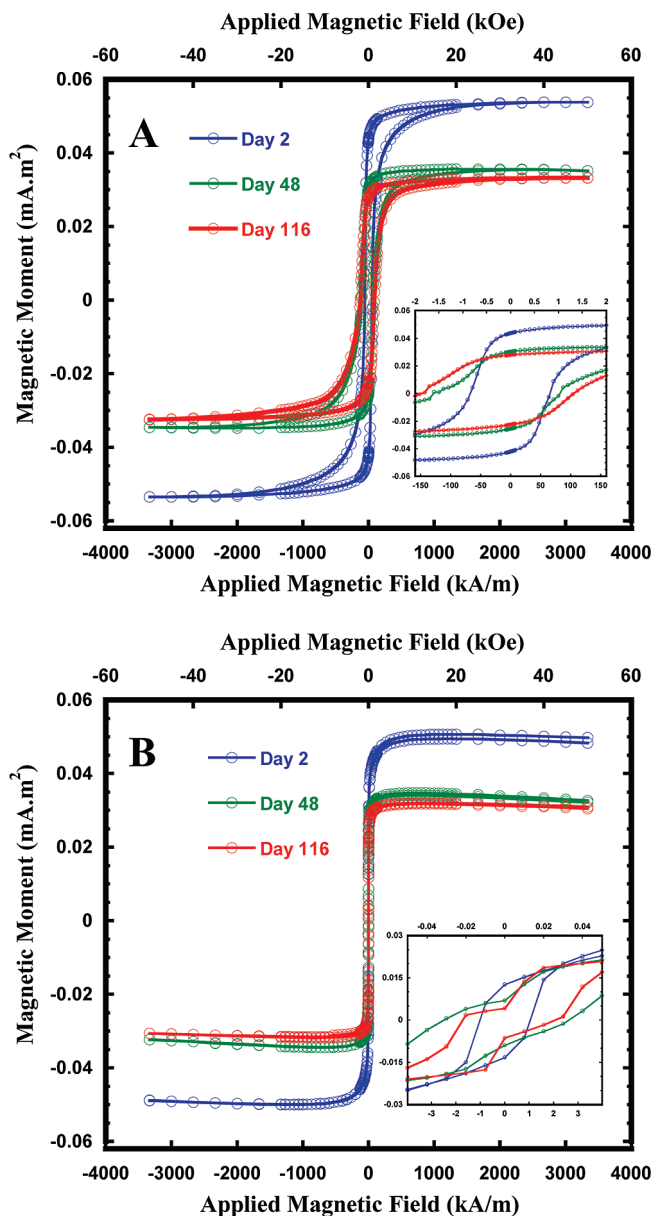


Figure 4. Hysteresis loops for the Co2 colloid measured on day 2, day 48, and day 116 after synthesis: (A) at 5 K with field cooling and (B) at 298 K. Insets show a close-up of the region around zero.

time. Here, we use the magnetic moment at 300 K with an applied magnetic field of 15.9 kA/m (200 Oe) (curve a), the magnetic moment at 300 K with an applied magnetic field of 39.8 kA/m (500 Oe) (curve b), and saturation magnetic moment at 298 K (curve c). As can be seen, over the first 46 day aging period of the Co2 colloid, the magnetic moment decreases by around 30%. Then over the following 68 day aging period of the Co2 colloid, the magnetic moment decreases by around 5%.

The hysteresis loops in Figure 4A were measured under field-cooled conditions where the sample was cooled from 298 to 5 K in an applied magnetic field of 3.98 MA/m (50 kOe) and then the hysteresis loop was measured at 5 K. Compared with the hysteresis loop for the Co2 colloid measured on day 2, the aged Co2 colloid also exhibits an obvious hysteresis loop shift and an increase in coercivity. An expanded plot is shown in the insert in Figure 4A for fields between -160 kA/m (-2 kOe) and $+160$ kA/m ($+2$ kOe). For the Co2 colloid measured on day 2, the hysteresis loop shift is negligible and the coercivity

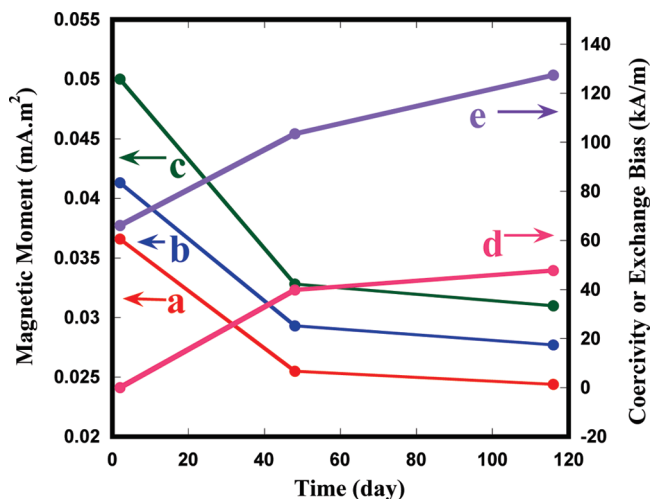


Figure 5. Magnetic moment, loop shift, and coercivity for the Co2 colloid as a function of aging time: (a) magnetic moment at 300 K with an applied magnetic field of 15.9 kA/m (200 Oe); (b) magnetic moment at 300 K with an applied magnetic field of 39.8 kA/m (500 Oe); (c) saturation magnetic moment at 298 K; (d) loop shift at 5 K; (e) coercivity at 5 K. The lines are guides to the eye.

is 66 kA/m (830 Oe). As the colloid ages, the hysteresis loop shift increases to 40 kA/m (500 Oe) on day 48 and 48 kA/m (600 Oe) on day 116, while the coercivity increases to 103 kA/m (1300 Oe) on day 48 and 127 kA/m (1600 Oe) on day 116. Curve d and curve e in Figure 5 summarize the loop shift and coercivity, respectively, for the Co2 colloid as a function of aging time. These trends correlate well with the ones for the magnetic moment.

Co nanocrystals coated with an fcc CoO were the first system where the hysteresis loop shift or exchange bias was observed.^{36–38} When the system is cooled down to below the Néel temperature of the AFM CoO (293 K)³⁹ in a magnetic field, the coupling at the AFM/FM CoO/Co interfaces imparts a unidirectional anisotropy to the Co cores, allowing them to be easily distinguished from pure Co nanocrystals via the appearance of an exchange bias. Above the Néel temperature, CoO is paramagnetic, and the exchange bias disappears.^{36–38} Thus at room temperature Co nanocrystals coated with CoO have magnetic properties similar to those of pure Co nanocrystals, but with a reduction in the saturation magnetic moment. Figure 4B shows the hysteresis loops at 298 K for the Co2 colloid measured on day 2, day 48, and day 116 after synthesis. As we can see from the expanded plot in the insert in Figure 4B for fields between -4 kA/m (-50 Oe) and $+4$ kA/m ($+50$ Oe), all three hysteresis loops are centered at the origin (no exchange bias). This contrasts nicely with the exchange bias shown in the hysteresis loops under field-cooled conditions at 5 K, strongly indicating the formation of the AFM/FM interfaces in the colloidal Co nanocrystals as the Co2 colloid ages.

However, CoO is not the only possible AFM oxide that can form. Co₃O₄ is also antiferromagnetic.²³ However, Co₃O₄ has a much lower Néel temperature, 40 K.³⁹ In our m vs T measurements, no peaks below 50 K have been observed to indicate the change between AFM and paramagnetic Co₃O₄.²³ Therefore, here, we believe that these AFM/FM interfaces are between fcc CoO and ϵ -Co. This is further supported by HRTEM on the aged Co2 colloidal nanocrystals.

Figure 6 shows a HRTEM image of a Co colloidal nanocrystal after aging in air for 70 days. The core of the nanocrystal (~ 10

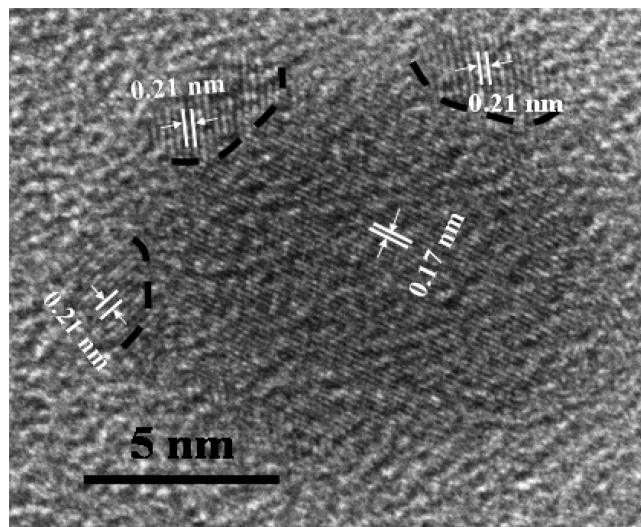


Figure 6. HRTEM image of an aged Co nanocrystal on day 70.

nm) still maintains a single crystalline structure. The d -spacing of lattice fringes for the core of the nanocrystal is 0.17 nm, comparable to that of the ϵ -phase Co (321) plane. As indicated in the image, three areas with different crystalline orientations can be clearly seen at the edge of the nanocrystal. The thickness of these areas is around 2 nm. However, the nanocrystal is not fully covered by a homogeneous crystalline shell and these three areas are scattered around the surface, indicating a nonuniform surface oxidation. The d -spacing of the lattice fringes for these three areas is 0.21 nm, close to the d -spacing value of the fcc CoO (200) plane. None of the crystalline Co₃O₄ planes has this d -spacing value, further confirming that the antiferromagnet formed on the ϵ -Co core is fcc CoO.

Since there is no detectable Co leaching for the aged colloid, assuming that uniform oxidation happens at the surface of a Co nanocrystal, the average thickness of the CoO shell can be estimated from the decrease in magnetic moment of the Co2 colloid over time as shown in Figure 5. We estimate the core size of a 10.5 nm ϵ -Co nanocrystal after losing 30% of its magnetic moment over the first 46 day aging to be 9.3 nm in diameter. This leaves a 0.6 nm thick shell of ϵ -Co to form the CoO shell. After the density change from ϵ -Co (8.635 g/cm³)¹⁸ into fcc CoO (6.44 g/cm³)⁴⁰ is taken into consideration, the particle has an ϵ -Co core of 9.3 nm and an fcc CoO shell of 0.95 nm. After the next 48 day aging, the particle has an ϵ -Co core of 9.1 nm and an fcc CoO shell of 1.1 nm. This demonstrates that the initial oxidation of Co nanocrystals is quick, and then the oxide grows more slowly. This is in agreement with the Cabrera–Mott theory on the oxidation of metals: after a rapid initial oxidation, further growth of the oxide is much slower.^{41–43}

Typically, the exchange bias would disappear if the AFM shell is thin enough.³⁸ This was confirmed recently on polycrystalline fcc Co nanocrystals (8 nm) where there is no exchange bias for a thin CoO shell (1.0 nm), but as the CoO shell thickens (3.2 nm), a low-temperature (below 50 K) paramagnetic behavior appears in m vs T measurements due to defects in the CoO shell and an exchange bias develops.²⁵ It is important to note that the polycrystalline fcc Co nanocrystals used there are dilute enough to render the interactions between the nanocrystals negligible. Another study on the magnetic properties of 4 nm fcc Co nanocrystals with a 1 nm fcc CoO shell has shown that there is no exchange bias for the dilute

and isolated nanocrystals, but that the compacted nanocrystals exhibit the features of exchange bias.⁴⁴ Further investigations on the same system have shown that as the coverage density of nanocrystals embedded in an aluminum oxide matrix increases from 3.5% to 15%, the superparamagnetic blocking temperature, the coercivity, and the loop shift radically increase.⁴⁵ This is a direct result of the interactions between CoO shells of the neighboring nanocrystals. As the coverage density increases, the interactions enhance the AFM/FM coupling, thus increasing the coercivity, the loop shift, and the magnetic stability of these core-shell nanocrystals.⁴⁵

In our system, even for the aged Co colloid on day 116, there is no sign of the low-temperature paramagnetic behavior due to defects in a thick CoO shell in Figure 3C.²⁵ The AFM CoO is thin and inhomogeneous. However, the FM Co core size is large (~10 nm) and colloidal nanocrystals tend to aggregate over time. Therefore, the magnetostatic coupling between neighboring Co cores is strong in the aged colloid, as evidenced by the m vs T curves in Figure 3 and the formation of induced chains under a small magnetic field at room temperature.²⁷ These results clearly indicate that the exchange bias observed in our system is not just due to the AFM/FM coupling within the same aged nanocrystal. Since there are no significant exchange interactions between different nanocrystals in the colloids, it is also a collective phenomenon, involving the significant magnetostatic interactions between different nanocrystals plus exchange interactions between the Co core and CoO layer within the same nanocrystal. When the Co cores are aligned due to the strong magnetostatic interactions and each core is exchange coupled to its CoO layer, then the CoO spins will have similar orientations in different nanocrystals. Under field-cooled conditions, the strong magnetostatic interactions between different nanocrystals enhance the AFM/FM exchange coupling between the fcc CoO and ϵ -Co to the point that loop shifts and increased coercivity are observed for the aged Co₂ colloid in Figure 4A.

Conclusion

TEM and magnetic measurements were combined to systematically characterize the growth of colloidal Co nanocrystals during synthesis and their subsequent stability in air. In the growth colloid, nanocrystals with an average size of 4.8 nm are produced and coexist with a paramagnetic component. This paramagnetic component is likely to be the Co cluster complexes produced during the growth of Co nanocrystals. The freshly prepared Co nanocrystals are monodisperse and have an average size of 10.5 nm. The disappearance of the earlier detected paramagnetic components in the growth colloids suggests the Co cluster complexes are fully converted into Co nanocrystals at the completion of synthesis. In the frozen colloids during and after synthesis, the thermal motion of colloidal nanocrystals, regardless of interaction strength, starts much earlier than the melting of the bulk liquid carrier. The initial local melting of liquid carrier, not the surface coating layer, is responsible for this early thermal motion. As the colloid ages, there is no detectable Co leaching into the liquid carrier and fcc CoO grows inhomogeneously onto the surface of these colloidal Co nanocrystals, resulting in a drop in the magnetic moment and an increase in the hysteresis loop shift and coercivity. The strong magnetostatic interactions between the neighboring nanocrystals enhance the AFM/FM exchange coupling between fcc CoO and

ϵ -Co and play a significant role in the exchange bias observed in the field-cooled hysteresis loops at 5 K.

Disclaimer

We identify certain commercial equipment, instruments, or materials in this article to specify adequately the experimental procedure. In no case does such identification imply recommendation or endorsement by the National Institute of Standards and Technology, nor does it imply that the materials or equipment identified are necessarily the best available for the purpose.

Acknowledgment. We acknowledge the help of Mr. Tiejun Zhang, Mr. Li-Chung Lai, and Dr. Wen-An Chiou in the Nanoscale Imaging Spectroscopy and Properties Laboratory (NISP) at the University of Maryland, College Park for TEM measurements.

References

- (1) Alivisatos, A. P. *Nat. Biotechnol.* **2004**, *22*, 47.
- (2) Burda, C.; Chen, X. B.; Narayanan, R.; El-Sayed, M. A. *Chem. Rev.* **2005**, *105*, 1025.
- (3) Daniel, M. C.; Astruc, D. *Chem. Rev.* **2004**, *104*, 293.
- (4) Wang, Z. L. *Characterization of nanophase materials*; Wiley-VCH: Weinheim; New York, 2000.
- (5) Peng, X. G.; Wickham, J.; Alivisatos, A. P. *J. Am. Chem. Soc.* **1998**, *120*, 5343–5344.
- (6) Chechik, V. *J. Am. Chem. Soc.* **2004**, *126*, 7780.
- (7) Jeong, U.; Teng, X. W.; Wang, Y.; Yang, H.; Xia, Y. N. *Adv. Mater.* **2007**, *19*, 33.
- (8) Leslie-Pelecky, D. L.; Rieke, R. D. *Chem. Mater.* **1996**, *8*, 1770.
- (9) Lu, A. H.; Salabas, E. L.; Schuth, F. *Angew. Chem., Int. Ed.* **2007**, *46*, 1222.
- (10) Majetich, S. A.; Sachan, M. *J. Phys. D: Appl. Phys.* **2006**, *39*, R407.
- (11) Dinega, D. P.; Bawendi, M. G. *Angew. Chem., Int. Ed.* **1999**, *38*, 1788.
- (12) Puentes, V. F.; Krishnan, K. M.; Alivisatos, A. P. *Science* **2001**, *291*, 2115.
- (13) Puentes, V. F.; Krishnan, K. M.; Alivisatos, A. P. *Appl. Phys. Lett.* **2001**, *78*, 2187.
- (14) Puentes, V. F.; Zanchet, D.; Erdonmez, C. K.; Alivisatos, A. P. *J. Am. Chem. Soc.* **2002**, *124*, 12874.
- (15) Yin, Y. D.; Rioux, R. M.; Erdonmez, C. K.; Hughes, S.; Somorjai, G. A.; Alivisatos, A. P. *Science* **2004**, *304*, 711.
- (16) Tripp, S. L.; Dunin-Borkowski, R. E.; Wei, A. *Angew. Chem., Int. Ed.* **2003**, *42*, 5591.
- (17) Carter, J. D.; Cheng, G. J.; Guo, T. *J. Phys. Chem. B* **2004**, *108*, 6901.
- (18) Diana, F. S.; Lee, S. H.; Petroff, P. M.; Kramer, E. J. *Nano Lett.* **2003**, *3*, 891.
- (19) de Silva, R. M.; Palshin, V.; Fronczek, F. R.; Hormes, J.; Kumar, C. *J. Phys. Chem. C* **2007**, *111*, 10320.
- (20) Lagunas, A.; Jimeno, C.; Font, D.; Sola, L.; Pericas, M. A. *Langmuir* **2006**, *22*, 3823.
- (21) Samia, A. C. S.; Hyzer, K.; Schlueter, J. A.; Qin, C. J.; Jiang, J. S.; Bader, S. D.; Lin, X. M. *J. Am. Chem. Soc.* **2005**, *127*, 4126.
- (22) Samia, A. C. S.; Schlueter, J. A.; Jiang, J. S.; Bader, S. D.; Qin, C. J.; Lin, X. M. *Chem. Mater.* **2006**, *18*, 5203.
- (23) Bao, Y. P.; Beerman, M.; Pakhomov, A. B.; Krishnan, K. M. *J. Phys. Chem. B* **2005**, *109*, 7220.
- (24) Tracy, J. B.; Bawendi, M. G. *Phys. Rev. B* **2006**, *74*, 184434.
- (25) Tracy, J. B.; Weiss, D. N.; Dinega, D. P.; Bawendi, M. G. *Phys. Rev. B* **2005**, *72*, 064404.
- (26) Cheng, G.; Dennis, C. L.; Shull, R. D.; Walker, A. R. H. *Langmuir* **2007**, *23*, 11740.
- (27) Cheng, G.; Romero, D.; Fraser, G. T.; Walker, A. R. H. *Langmuir* **2005**, *21*, 12055.
- (28) Cheng, G.; Carter, J. D.; Guo, T. *Chem. Phys. Lett.* **2004**, *400*, 122.
- (29) Butter, K.; Bomans, P. H. H.; Frederik, P. M.; Vroege, G. J.; Philipse, A. P. *Nat. Mater.* **2003**, *2*, 88.
- (30) Klokkenburg, M.; Vonk, C.; Claesson, E. M.; Meeldijk, J. D.; Erne, B. H.; Philipse, A. P. *J. Am. Chem. Soc.* **2004**, *126*, 16706.
- (31) Klokkenburg, M.; Erne, B. H.; Philipse, A. P. *Langmuir* **2005**, *21*, 1187.

- (32) Holland, G. F.; Ellis, D. E.; Tyler, D. R.; Gray, H. B.; Trogler, W. C. *J. Am. Chem. Soc.* **1987**, *109*, 4276.
- (33) Pachon, L. D.; Rothenberg, G. *Appl. Organomet. Chem.* **2008**, *22*, 288.
- (34) Gaikwad, A. V.; Holuigue, A.; Thathagar, M. B.; ten Elshof, J. E.; Rothenberg, G. *Chem.—Eur. J.* **2007**, *13*, 6908.
- (35) de Vries, J. G. *Dalton Trans.* **2006**, (3), 421.
- (36) Meiklejohn, W. H.; Bean, C. P. *Phys. Rev.* **1956**, *102*, 1413.
- (37) Meiklejohn, W. H.; Bean, C. P. *Phys. Rev.* **1957**, *105*, 904.
- (38) Nogues, J.; Schuller, I. K. *J. Magn. Magn. Mater.* **1999**, *192*, 203.
- (39) Lide, D. R. *CRC handbook of chemistry and physics*; CRC: Boca Raton, FL, 2008.
- (40) Du Trémolet de Lacheisserie, E.; Gignoux, D.; Schlenker, M. *Magnetism*; Kluwer Academic Publishers: Norwell, MA, 2002.
- (41) Mott, N. F. *Trans. Faraday Soc.* **1940**, *35*, 0472.
- (42) Chernavskii, P. A.; Pankina, G. V.; Chernavskii, A. P.; Peskov, N. V.; Afanasiev, P.; Perov, N. S.; Tennyov, V. A. *J. Phys. Chem. C* **2007**, *111*, 5576.
- (43) Wang, C. M.; Baer, D. R.; Thomas, L. E.; Amonette, J. E.; Antony, J.; Qiang, Y.; Duscher, G. *J. Appl. Phys.* **2005**, *98*, 094308.
- (44) Skumryev, V.; Stoyanov, S.; Zhang, Y.; Hadjipanayis, G.; Givord, D.; Nogues, J. *Nature* **2003**, *423*, 850.
- (45) Nogues, J.; Skumryev, V.; Sort, J.; Stoyanov, S.; Givord, D. *Phys. Rev. Lett.* **2006**, *97*, 157203.

CG900426J